Search for Transient Astrophysical Neutrino Emission with IceCube-DeepCore

IceCube Collaboration: M. G. Aartsen[1], K. Abraham[2], M. Ackermann[3], J. Adams[4],

J. A. Aguilar[5], M. Ahlers[6], M. Ahrens[7], D. Altmann[8], T. Anderson[9], I. Ansseau[5],

M. Archinger[10], C. Arguelles[6], T. C. Arlen[9], J. Auffenberg[11], X. Bai[12], S. W. Barwick[13],

V. Baum[10], R. Bay[14], J. J. Beatty[15,16], J. Becker Tjus[17], K.-H. Becker[18], E. Beiser[6],

S. BenZvi[6], P. Berghaus[3], D. Berley[19], E. Bernardini[3], A. Bernhard[2], D. Z. Besson[20],

G. Binder[21,14], D. Bindig[18], M. Bissok[11], E. Blaufuss[19], J. Blumenthal[11], D. J. Boersma[22],

C. Bohm[7], M. Börner[23], F. Bos[17], D. Bose[24], S. Böser[10], O. Botner[22], J. Braun[6],

L. Brayeur[25], H.-P. Bretz[3], N. Buzinsky[26], J. Casey[27], M. Casier[25], E. Cheung[19],

D. Chirkin[6], A. Christov[28], K. Clark[29], L. Classen[8], S. Coenders[2], D. F. Cowen[9,30],

A. H. Cruz Silva[3], J. Daughhetee[27], J. C. Davis[15], M. Day[6], J. P. A. M. de André[31],

C. De Clercq[25], E. del Pino Rosendo[10], H. Dembinski[32], S. De Ridder[33], P. Desiati[6],

K. D. de Vries[25], G. de Wasseige[25], M. de With[34], T. DeYoung[31], J. C. Díaz-Vélez[6],

V. di Lorenzo[10], J. P. Dumm[7], M. Dunkman[9], R. Eagan[9], B. Eberhardt[10], T. Ehrhardt[10],

B. Eichmann[17], S. Euler[22], P. A. Evenson[32], O. Fadiran[6], S. Fahey[6], A. R. Fazely[35],

A. Fedynitch[17], J. Feintzeig[6], J. Felde[19], K. Filimonov[14], C. Finley[7], T. Fischer-Wasels[18],

S. Flis[7], C.-C. Fösig[10], T. Fuchs[23], T. K. Gaisser[32], R. Gaior[36], J. Gallagher[37],

L. Gerhardt[21,14], K. Ghorbani[6], D. Gier[11], L. Gladstone[6], M. Glagla[11], T. Glüsenkamp[3],

A. Goldschmidt[21], G. Golup[25], J. G. Gonzalez[32], D. Góra[3], D. Grant[26], J. C. Groh[9],

A. Groß[2], C. Ha[21,14], C. Haack[11], A. Haj Ismail[33], A. Hallgren[22], F. Halzen[6],

B. Hansmann[11], K. Hanson[6], D. Hebecker[34], D. Heereman[5], K. Helbing[18], R. Hellauer[19],

D. Hellwig[11], S. Hickford[18], J. Hignight[31], G. C. Hill[1], K. D. Hoffman[19], R. Hoffmann[18],

K. Holzapfel[2], A. Homeier[38], K. Hoshina[6,49], F. Huang[9], M. Huber[2], W. Huelsnitz[19],

P. O. Hulth[7], K. Hultqvist[7], S. In[24], A. Ishihara[36], E. Jacobi[3], G. S. Japaridze[39], K. Jero[6],

M. Jurkovic[2], B. Kaminsky[3], A. Kappes[8], T. Karg[3], A. Karle[6], M. Kauer[6,40], A. Keivani[9],

27   J. L. Kelley[6], J. Kemp[11], A. Kheirandish[6], J. Kiryluk[41], J. Kläs[18], S. R. Klein[21,14],

28   G. Kohnen[42], R. Koirala[32], H. Kolanoski[34], R. Konietz[11], A. Koob[11], L. Köpke[10],

29   C. Kopper[26], S. Kopper[18], D. J. Koskinen[43], M. Kowalski[34,3], K. Krings[2], G. Kroll[10],

30   M. Kroll[17], J. Kunnen[25], N. Kurahashi[44], T. Kuwabara[36], M. Labare[33], J. L. Lanfranchi[9],

31   M. J. Larson[43], M. Lesiak-Bzdak[41], M. Leuermann[11], J. Leuner[11], J. Lünemann[10],

32   J. Madsen[45], G. Maggi[25], K. B. M. Mahn[31], R. Maruyama[40], K. Mase[36], H. S. Matis[21],

33   R. Maunu[19], F. McNally[6], K. Meagher[5], M. Medici[43], A. Meli[33], T. Menne[23], G. Merino[6],

34   T. Meures[5], S. Miarecki[21,14], E. Middell[3], E. Middlemas[6], J. Miller[25], L. Mohrmann[3],

35   T. Montaruli[28], R. Morse[6], R. Nahnhauer[3], U. Naumann[18], H. Niederhausen[41],

36   S. C. Nowicki[26], D. R. Nygren[21], A. Obertacke[18], A. Olivas[19], A. Omairat[18],

37   A. O'Murchadha[5], T. Palczewski[46], H. Pandya[32], L. Paul[11], J. A. Pepper[46],

38   C. Pérez de los Heros[22], C. Pfendner[15], D. Pieloth[23], E. Pinat[5], J. Posselt[18], P. B. Price[14],

39   G. T. Przybylski[21], J. Pütz[11], M. Quinnan[9], C. Raab[5], L. Rädel[11], M. Rameez[28],

40   K. Rawlins[47], R. Reimann[11], M. Relich[36], E. Resconi[2], W. Rhode[23], M. Richman[44],

41   S. Richter[6], B. Riedel[26], S. Robertson[1], M. Rongen[11], C. Rott[24], T. Ruhe[23],

42   D. Ryckbosch[33], S. M. Saba[17], L. Sabbatini[6], H.-G. Sander[10], A. Sandrock[23], J. Sandroos[10],

43   S. Sarkar[43,48], K. Schatto[10], F. Scheriau[23], M. Schimp[11], T. Schmidt[19], M. Schmitz[23],

44   S. Schoenen[11], S. Schöneberg[17], A. Schönwald[3], L. Schulte[38], D. Seckel[32], S. Seunarine[45],

45   R. Shanidze[3], M. W. E. Smith[9], D. Soldin[18], M. Song[19], G. M. Spiczak[45], C. Spiering[3],

46   M. Stahlberg[11], M. Stamatikos[15,50], T. Stanev[32], N. A. Stanisha[9], A. Stasik[3],

47   T. Stezelberger[21], R. G. Stokstad[21], A. Stößl[3], E. A. Strahler[25], R. Ström[22],

48   N. L. Strotjohann[3], G. W. Sullivan[19], M. Sutherland[15], H. Taavola[22], I. Taboada[27],

49   S. Ter-Antonyan[35], A. Terliuk[3], G. Tešić[9], S. Tilav[32], P. A. Toale[46], M. N. Tobin[6], D. Tosi[6],

50   M. Tselengidou[8], A. Turcati[2], E. Unger[22], M. Usner[3], S. Vallecorsa[28], J. Vandenbroucke[6],

51   N. van Eijndhoven[25], S. Vanheule[33], J. van Santen[6], J. Veenkamp[2], M. Vehring[11],

52   M. Voge[38], M. Vraeghe[33], C. Walck[7], A. Wallace[1], M. Wallraff[11], N. Wandkowsky[6],

53   Ch. Weaver[26], C. Wendt[6], S. Westerhoff[6], B. J. Whelan[1], N. Whitehorn[6], C. Wichary[11],

54   K. Wiebe[10], C. H. Wiebusch[11], L. Wille[6], D. R. Williams[46], H. Wissing[19], M. Wolf[7],

55   T. R. Wood[26], K. Woschnagg[14], D. L. Xu[46], X. W. Xu[35], Y. Xu[41], J. P. Yanez[3], G. Yodh[13],

56   S. Yoshida[36], and M. Zoll[7]

[1]Department of Physics, University of Adelaide, Adelaide, 5005, Australia

[2]Technische Universität München, D-85748 Garching, Germany

[3]DESY, D-15735 Zeuthen, Germany

[4]Dept. of Physics and Astronomy, University of Canterbury, Private Bag 4800, Christchurch, New Zealand

[5]Université Libre de Bruxelles, Science Faculty CP230, B-1050 Brussels, Belgium

[6]Dept. of Physics and Wisconsin IceCube Particle Astrophysics Center, University of Wisconsin, Madison, WI 53706, USA

[7]Oskar Klein Centre and Dept. of Physics, Stockholm University, SE-10691 Stockholm, Sweden

[8]Erlangen Centre for Astroparticle Physics, Friedrich-Alexander-Universität Erlangen-Nürnberg, D-91058 Erlangen, Germany

[9]Dept. of Physics, Pennsylvania State University, University Park, PA 16802, USA

[10]Institute of Physics, University of Mainz, Staudinger Weg 7, D-55099 Mainz, Germany

[11]III. Physikalisches Institut, RWTH Aachen University, D-52056 Aachen, Germany

[12]Physics Department, South Dakota School of Mines and Technology, Rapid City, SD 57701, USA

[13]Dept. of Physics and Astronomy, University of California, Irvine, CA 92697, USA

[14]Dept. of Physics, University of California, Berkeley, CA 94720, USA

[15]Dept. of Physics and Center for Cosmology and Astro-Particle Physics, Ohio State University, Columbus, OH 43210, USA

[16]Dept. of Astronomy, Ohio State University, Columbus, OH 43210, USA

[17]Fakultät für Physik & Astronomie, Ruhr-Universität Bochum, D-44780 Bochum, Germany

[18]Dept. of Physics, University of Wuppertal, D-42119 Wuppertal, Germany

[19]Dept. of Physics, University of Maryland, College Park, MD 20742, USA

^{20}Dept. of Physics and Astronomy, University of Kansas, Lawrence, KS 66045, USA

^{21}Lawrence Berkeley National Laboratory, Berkeley, CA 94720, USA

^{22}Dept. of Physics and Astronomy, Uppsala University, Box 516, S-75120 Uppsala, Sweden

^{23}Dept. of Physics, TU Dortmund University, D-44221 Dortmund, Germany

^{24}Dept. of Physics, Sungkyunkwan University, Suwon 440-746, Korea

^{25}Vrije Universiteit Brussel, Dienst ELEM, B-1050 Brussels, Belgium

^{26}Dept. of Physics, University of Alberta, Edmonton, Alberta, Canada T6G 2E1

^{27}School of Physics and Center for Relativistic Astrophysics, Georgia Institute of Technology, Atlanta, GA 30332, USA

^{28}Département de physique nucléaire et corpusculaire, Université de Genève, CH-1211 Genève, Switzerland

^{29}Dept. of Physics, University of Toronto, Toronto, Ontario, Canada, M5S 1A7

^{30}Dept. of Astronomy and Astrophysics, Pennsylvania State University, University Park, PA 16802, USA

^{31}Dept. of Physics and Astronomy, Michigan State University, East Lansing, MI 48824, USA

^{32}Bartol Research Institute and Dept. of Physics and Astronomy, University of Delaware, Newark, DE 19716, USA

^{33}Dept. of Physics and Astronomy, University of Gent, B-9000 Gent, Belgium

^{34}Institut für Physik, Humboldt-Universität zu Berlin, D-12489 Berlin, Germany

^{35}Dept. of Physics, Southern University, Baton Rouge, LA 70813, USA

^{36}Dept. of Physics, Chiba University, Chiba 263-8522, Japan

^{37}Dept. of Astronomy, University of Wisconsin, Madison, WI 53706, USA

^{38}Physikalisches Institut, Universität Bonn, Nussallee 12, D-53115 Bonn, Germany

^{39}CTSPS, Clark-Atlanta University, Atlanta, GA 30314, USA

^{40}Dept. of Physics, Yale University, New Haven, CT 06520, USA

⁴¹Dept. of Physics and Astronomy, Stony Brook University, Stony Brook, NY 11794-3800, USA

⁴²Université de Mons, 7000 Mons, Belgium

⁴³Niels Bohr Institute, University of Copenhagen, DK-2100 Copenhagen, Denmark

⁴⁴Dept. of Physics, Drexel University, 3141 Chestnut Street, Philadelphia, PA 19104, USA

⁴⁵Dept. of Physics, University of Wisconsin, River Falls, WI 54022, USA

⁴⁶Dept. of Physics and Astronomy, University of Alabama, Tuscaloosa, AL 35487, USA

⁴⁷Dept. of Physics and Astronomy, University of Alaska Anchorage, 3211 Providence Dr., Anchorage, AK 99508, USA

⁴⁸Dept. of Physics, University of Oxford, 1 Keble Road, Oxford OX1 3NP, UK

⁴⁹Earthquake Research Institute, University of Tokyo, Bunkyo, Tokyo 113-0032, Japan

⁵⁰NASA Goddard Space Flight Center, Greenbelt, MD 20771, USA

ABSTRACT

We present the results of a search for astrophysical sources of brief transient neutrino emission using IceCube and DeepCore data acquired between May 15th 2012 and April 30th 2013. While the search methods employed in this analysis are similar to those used in previous IceCube point source searches, the data set being examined consists of a sample of predominantly sub-TeV muon neutrinos from the Northern Sky (-5° < δ < 90°) obtained through a novel event selection method. This search represents a first attempt by IceCube to identify astrophysical neutrino sources in this relatively unexplored energy range. The reconstructed direction and time of arrival of neutrino events is used to search for any significant self-correlation in the dataset. The data revealed no significant source of transient neutrino emission. This result has been used to construct limits on generic soft-spectra transients as well as a specific model of neutrino emission from soft jets in core-collapse supernovae.

Subject headings: neutrino astronomy, neutrinos, GRB, supernova, astroparticle physics

1. Introduction

The nascent field of high-energy neutrino astronomy opens the possibility of answering several open questions in astrophysics due in large part to the neutrino's ability to escape the densest regions of astrophysical environments. Specifically, the detection of transient astrophysical neutrino sources will help shed light on the acceleration mechanisms at work in some of the most energetic phenomena in the Universe such as gamma-ray bursts, supernovae, and active galactic nuclei. Previous attempts to detect such sources with the IceCube Neutrino Observatory (IceCube Collaboration et al. 2006) are most sensitive to neutrino fluxes above 1 TeV with poor sensitivity below 100 GeV. Searches for astrophysical sources at lower energies (1–100 GeV) have been performed by Super-Kamiokande (Thrane et al. 2009), however the detector's 50 kton instrumented volume limits its sensitivity to astrophysical neutrino fluxes. A newly developed 30–300 GeV muon neutrino sample collected by IceCube and its low energy extension DeepCore (Abbasi et al. 2012) enhances IceCube's sensitivity in this under-explored energy range. In this paper we will present the results of a search for transient neutrino emission in this GeV-scale neutrino sample.

The detection of astrophysical neutrino sources is a primary design goal of the IceCube Neutrino Observatory (IceCube Collaboration et al. 2006). Located at the geographic South Pole, IceCube utilizes the clear Antarctic glacial ice ice cap as a detection medium for the Cherenkov light produced by secondary products of neutrino interactions. The detector consists of 5,160 Digital Optical Modules (DOMs) distributed among 86 cables or "strings" to form a 1 km^3 instrumented volume. These DOMs house photomultiplier tubes (PMTs), to detect Cherenkov photons, as well as digitizing electronics for initial processing of the PMT data. A centrally located region of denser instrumentation featuring DOMs with more sensitive PMTs comprises the DeepCore sub-array. This extension to the IceCube array enhances the detector's response to lower energy neutrino events.

Typical searches for astrophysical sources with IceCube make use of a sample primarily comprised of an irreducible background of high-energy atmospheric muon neutrinos ($E_\nu \gtrsim 1$ TeV) to look for both steady (Aartsen et al. 2014b) and transient sources (Aartsen et al. 2015). As of yet, these searches have not found any significant self-correlations within the data sample nor correlations between the neutrino data and known astrophysical objects of interest. So far, these analyses have largely eschewed low energy neutrino events collected by DeepCore for two reasons. First, the poorer angular resolution of these events renders them less suitable for pointing analyses. Second, the soft spectrum of the atmospheric neutrino flux results in higher rate of background neutrino events. However, the increased background can be somewhat mitigated by searching solely for transient sources. Therefore, applying previously developed search techniques (Braun et al. 2010) to a sample of low energy ($30\ \mathrm{GeV} \leq E_\nu < 300\ \mathrm{GeV}$) muon neutrino events from DeepCore can enhance IceCube's sensitivity to short transient neutrino sources with softer spectra.

Due to the large atmospheric neutrino background in this energy range, searches using a data set composed of these low energy events will only be sensitive to emission timescales on the order of one day or shorter. Active galactic nuclei (AGN) undergoing flaring events are one potential source for emission on this timescale. Protons may be accelerated in relativistic jets, powered by accretion onto the AGN, resulting in the production of pions (and subsequently neutrinos) in shocks due to proton-photon interactions and proton self-collisions (Becker & Biermann 2009). Brief periods of enhanced accretion would then result in a commensurate increase in the neutrino flux from the AGN, which may be detectable using time-dependent search methods. Sub-photospheric neutrino emission from gamma-ray bursts (GRBs) represents another possible source for this search. A model for photospheric gamma-ray emission in GRBs by Murase et al. (2013) suggests that a substantial flux of 100 GeV-scale neutrinos may be produced during the initial stages of relativistic outflow in the GRB. Decoupling of protons and neutrons during the initial

113 formation of the relativistic jet causes hadronuclear collisions resulting in the production

114 of pions and the production of neutrinos via pion decay. The predicted energy for the

115 neutrinos produced in these sub-photospheric collisions is on the order of 100 GeV, and

116 therefore this GRB neutrino flux may only be visible to IceCube searches with the inclusion

117 of sub-TeV neutrino events.

118 Perhaps the most promising potential source for this study is a special class of

119 core-collapse supernova referred to as choked GRBs (Mészáros & Waxman 2001). The

120 standard GRB model assumes that relativistic jets are generated during the accretion of

121 material onto the compact object formed during core-collapse (Rees & Meszaros 1992).

122 Fermi-acceleration of charged particles occurs within the internal shocks of these jets leading

123 to gamma ray emission once the jets breach the surrounding stellar envelope. There is an

124 observed correlation between long duration GRBs and core-collapse supernovae (CC SNe)

125 ((Woosley & Bloom 2006), (Modjaz 2011)). While the observed fraction of SNe resulting in

126 the occurrence of a GRB is quite low, it may be that a larger fraction of core-collapse SNe

127 still manage to produce mildly relativistic jets. Due to insufficient energy, these jets fail

128 to break through the stellar envelope and any gamma ray emission is effectively 'choked'

129 off. If protons are accelerated in these jets, then neutrino production will occur in the

130 shocks of the jet irrespective of whether or not the jet successfully escapes. A model of

131 this neutrino emission proposed by Razzaque et al. (2004) and extended upon by Ando &

132 Beacom (2005), hereafter referred to as the RMW/AB model, suggests that these neutrinos

133 may be detectable by IceCube-DeepCore for nearby supernovae (Taboada 2010).

134 We present the results of a search for transient neutrino emission with a set of

135 low-energy neutrino event data collected from May 15th, 2012 to April 30th, 2013. The

136 data selection methods used to acquire this unique event sample will be detailed in Sec. 2.

137 Analysis methods and search techniques are discussed in Sec. 3. Finally, the results of the

138 search are given in Sec. 4 in addition to how these results may be interpreted within the
139 context of generic neutrino flares as well as choked GRBs under the RMW/AB model.

2.   Event Selection

141   The data acquisition process begins with the fulfillment of one of three trigger conditions
142 that prompt the readout of the detector data. Each of these triggers requires some number
143 of DOMs to exhibit hard local coincidence (HLC) within a defined time window. To satisfy
144 the HLC condition, two or more neighboring (or next-to-nearest-neighboring) DOMs on the
145 same string must register photon hits within a ± 1 μs window. The trigger for the lowest
146 energy events (often referred to as simple majority trigger 3 or SMT3) requires three HLC
147 DOM hits within a time window of 2.5 μs among the DeepCore string DOMs (or in DOMs
148 on IceCube strings neighboring DeepCore). The two other triggers that serve as input for
149 this event selection operate over the entire detector array with one requiring eight HLC
150 DOM hits in a 5 μs window (SMT8) and the other requiring four HLC DOM hits within a
151 cylinder of height of 75m and a radius of 175m in a 1 μs window (Cylinder Trigger).

152   Events satisfying these trigger conditions are then passed to the DeepCore data filter
153 (Abbasi et al. 2012). This filter reduces the number of cosmic ray muons by using the outer
154 regions of the detector as an active veto to tag down-going events originating outside the
155 detector. Specifically, the filter examines timing and position information of DOM hits
156 inside the DeepCore fiducial volume to identify a center of gravity (CoG) or vertex. For
157 each DOM hit in the veto region, the speed of a hypothetical particle connecting that veto
158 region hit to the CoG inside the fiducial volume is calculated. Veto regions hits whose
159 speed lies within a range consistent with that of the speed of light are causally related and
160 are therefore likely the product of background cosmic ray muons. Events having more than
161 one correlated veto region hit are removed by the filter.

162 During the observation period of this search, the DeepCore filter consisted of two

163 separate branches characterized by differing definitions of fiducial and veto volumes as

164 opposed to the single definition given in Abbasi et al. (2012). Another key difference of the

165 applied filter, with respect to the definition provided in Abbasi et al. (2012), is that it now

166 makes use of some isolated DOM hit information instead of only using HLC hits. Events

167 satisfying the SMT3 trigger feed the standard DeepCore filter branch whose fiducial and

168 veto region definitions are roughly equivalent to those described in Abbasi et al. (2012).

169 The SMT8 and Cylinder Trigger events, in addition to SMT3 events that fail the standard

170 filter branch, feed into the other branch of the filter which makes use of a more relaxed

171 veto region, consisting of two instead of three layers of IceCube strings, providing a larger

172 detection volume. The output of both branches of this filter are used in this search with

173 the standard three-layer veto focusing on low-energy events and the two-layer veto branch

174 retaining higher energy events. These branches are referred to as the low-energy stream

175 (LES) and high-energy stream (HES) and have an exclusive event rate of 17.3 Hz and 23.3

176 Hz, respectively.

2.1. Veto Cuts and Event Reconstruction

178 Events belonging to both the LES and HES are subjected to several cuts that make

179 use of veto region hit information, event topology, and event reconstructions to reduce

180 the volume of cosmic ray background events as well as eliminate events that are the

181 result of PMT dark noise-induced triggering. The first of these cuts requires at least

182 two DeepCore DOM hits within a 250 ns window to remove SMT3 events that are the

183 result of spurious hits. An algorithm designed to search for track-like events is then

184 used to eliminate noise-induced events that show little evidence of correlation in DOM

185 hits. Additionally, events are required to have at least 10 hit DOMs, to allow for a

– 13 –

well-constrained reconstruction. The DeepCore filter algorithm is also reapplied several times using looser DOM hit cleaning settings to allow more isolated DOM hits in the veto region to contribute to the vertex calculations. Finally, the number of DOM hits that occur prior to the first hit inside the DeepCore detection volume is used as a cut parameter to eliminate potential cosmic ray muon events missed by the filter.

The initial event reconstruction uses a simple linear fit (Aartsen et al. 2014a) to determine the first-guess direction of a muon track that describes the observed DOM hit pattern. This linear reconstruction is then used as a seed for a likelihood-based reconstruction (Ahrens et al. (2004)) which uses a single-photoelectron (SPE) hypothesis to describe the probability of DOMs receiving light from the track at a given time due to scattering in the ice. Six iterations of the SPE likelihood reconstruction are performed to obtain a best-fit track for the event. Any event with a reconstructed direction, from either the linear or SPE likelihood fit, more than $5°$ above the horizon is removed from the sample. We also require that the angular separation between these two reconstructions is less than $30°$ for events in the HES sample.

Spurious DOM hits that occur in the central detector prior to the arrival of cosmic ray muons allow many background events to elude detection through the standard veto technique. To isolate these events, a separate SPE likelihood reconstruction is performed without using any information from the first two DOM hits in the event. Just as before, events with a reconstructed direction more than $5°$ above the horizon are removed. Events in the LES portion of the sample are disproportionately affected by noise hits due to both the lower light yield of these events as well as the increased noise rate of the higher quantum efficiency DeepCore DOMs. An additional SPE likelihood reconstruction is performed for LES events that attempts to mitigate the noise contribution to the likelihood by requiring isolated DOM hits to be more strongly correlated to hits satisfying the HLC condition.

Once again, if the best-fit direction from this additional reconstruction on LES events is 5°
above the horizon, the event is removed.

A final event reconstruction uses the previously mentioned six iteration SPE likelihood
fit as its seed. This reconstruction differs from the seed in two important ways. First, it
uses a multi-photoelectron likelihood (MPE) instead of the simpler SPE algorithm used
previously (see Ahrens et al. (2004)). Second, a parameterization of Monte Carlo simulation
of photon transport is used in place of an analytic approximation to model the timing
distribution for the arrival of Cherenkov photons to the DOM PMTs (Whitehorn et al.
2013). This reconstruction is identical to that used in a multi-year point source search
with IceCube (Aartsen et al. 2014b) and the results of this fit are used for the final data
analysis. In order to estimate the angular uncertainty of the reconstruction, the likelihood
space about the reconstructed direction is fit with a paraboloid via the method described
in Neunhöffer (2006). The angular uncertainty derived from the paraboloid method serves
as event quality parameter, and only events having an estimated angular error σ_i less than
45° are kept.

2.2. Boosted Decision Tree

After the application of the described veto and reconstruction cuts, the ability to
separate the muon background from potential neutrino signal events via simple cuts is
drastically reduced. We therefore use a boosted decision tree (BDT) in order to isolate
a final sample with acceptable neutrino purity, i.e. $< 10\%$ of events are the result of
background cosmic ray muons. At this level of event selection, the large majority of
experimental data still consists of background cosmic ray muons allowing the actual data
to serve as a background training sample for the BDT. Simulated neutrino signal events
belonging to the LES or HES branches exhibit significant differences in the distribution of

– 15 –

₂₃₅ the input BDT parameters, described below, necessitating the construction of two separate

₂₃₆ BDTs.

₂₃₇   The event parameters used for the LES tree include the location of the reconstructed

₂₃₈ event vertex, the number of 'direct' DOM hits (featuring a photon travel time residual

₂₃₉ between -25 and 150 ns with respect to the reconstructed muon track), the reduced

₂₄₀ log-likelihood of the MPE reconstruction, the average distance between DOM hits and the

₂₄₁ reconstructed track weighted by DOM PMT charge, and the highest clustering of veto

₂₄₂ region PMT charge (found by brute force reconstruction methods). The HES BDT makes

₂₄₃ use of the direct hits parameter described above, the reduced log-likelihood of the MPE

₂₄₄ reconstruction, the average charge-weighted DOM distance to track, and the best fit track

₂₄₅ length using information from direct DOM hits. A simulated signal neutrino event sample

weighted to a $E^{-2.5}$ (LES) or E^{-2} (HES) spectrum is used for signal training.
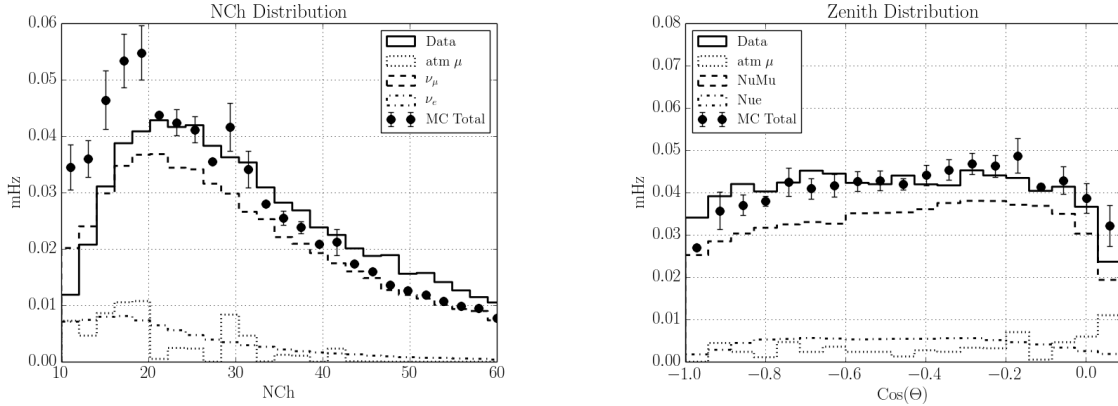
Fig. 1.— Final event rate distributions for the number of DOMs registering hits during the
event (left) and the cosine of the reconstructed event zenith in detector coordinates (right).

₂₄₆

₂₄₇   Events are then input to the trained BDT, and a cut on the event BDT score is

₂₄₈ imposed to yield a data sample featuring a neutrino purity of approximately 90%. This

₂₄₉ final event sample consists of 22,040 events over a livetime of ∼330 days, corresponding to a

data rate of about 0.77 mHz. As Figure 1 indicates, the final sample is mostly composed of atmospheric neutrinos with an estimated cosmic ray muon contamination of approximately 0.07 mHz. There is some disagreement between the predictions from simulation and the actual data (primarily the rate of events featuring a low number of DOM hits), and much of this discrepancy stems from limited statistics for cosmic ray muon simulation. This limitation is overcome by measuring the background directly from the final data set itself.

The neutrino effective area for this event selection is shown in Figure 2. While standard IceCube analyses clearly have superior sensitivity at higher energies, this event selection shows increased acceptance for events below about 100 GeV in neutrino energy. Figure 2 also shows the angular resolution for events at the analysis level as a function of energy. Lower neutrino energies result in muon tracks that are both shorter and dimmer, leading to difficulty in resolving the direction of the neutrino primary. The kinematic angle between the neutrino primary and muon secondary also contributes to the angular error. The median kinematic muon-neutrino angle after event selection ranges from $\sim 3°$ at 50 GeV to $\sim 1°$ at 300 GeV. As Figure 2 shows, the efficacy of the reconstruction method used in this analysis begins to deteriorate rapidly below 30 GeV due to too few DOM hits. Although the pointing ability of these low-energy neutrino events is limited, they are still able to contribute to the search through temporal correlation with other events in the sample.

3.   Analysis Method

The search methods employed in the analysis of this data are nearly identical to those used in previous time-dependent IceCube analyses (see Braun et al. (2008) and Aartsen et al. (2015)). The arrival times and directions of events within the dataset are input to a likelihood function which is then used to perform a likelihood ratio test to compare a signal plus background hypothesis for the data to the background only hypothesis.
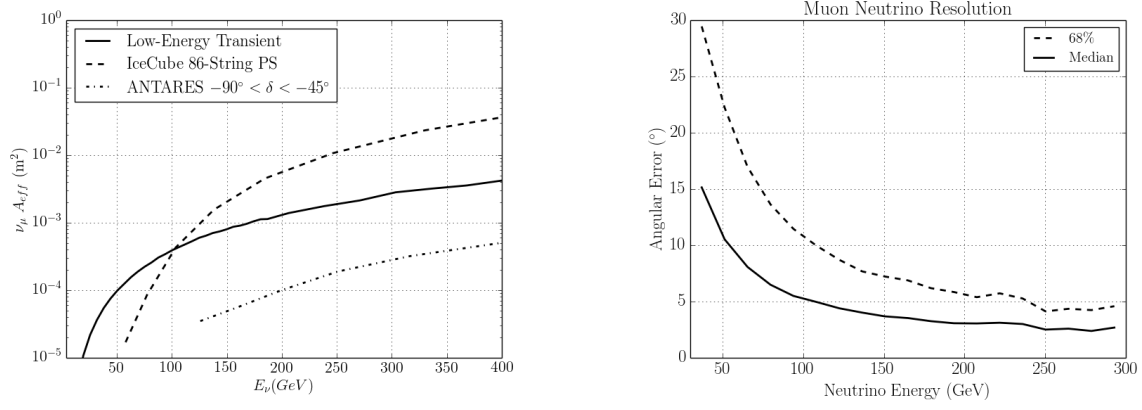
Fig. 2.— (left) The muon neutrino effective area as a function of neutrino energy for the presented search. The effective areas for both the 4 year IceCube point source search (Aartsen et al. 2014b) and the 4 year ANTARES point source search (Adrián-Martínez et al. 2012) are plotted as well for comparison. (right) Angular resolution as a function of energy after event selection.

Construction of this likelihood function begins with the assignment of individual event probabilities that reflect the likelihood of seeing an event i with arrival time t_i, reconstructed direction $\mathbf{x}_i$, and angular uncertainty σ_i given a hypothetical source located at $\mathbf{x}_s$ with strength n_s having a Gaussian time profile with mean time t_0 and width σ_w.

$$\mathcal{P}_i(\mathbf{x}_i, t_i, \sigma_i | \mathbf{x}_s, n_s, t_0, \sigma_w) = \frac{n_s}{n_{\text{tot}}} \mathcal{S}_i + \left(1 - \frac{n_s}{n_{\text{tot}}}\right) \mathcal{B}_i \tag{1}$$

The $\mathcal{S}_i$ and $\mathcal{B}_i$ terms listed in Eq. 1 are the signal and background probability density functions (p.d.f.) respectively. The p.d.f.s used in this search differ slightly from those in previously reported searches in that they use no reconstructed energy information. The signal p.d.f. is given by

$$\mathcal{S}_i(|\mathbf{x}_i - \mathbf{x}_s|, t_i, t_o, \sigma_w, \sigma_i) = S_i(|\mathbf{x}_i - \mathbf{x}_s|, \sigma_i) \cdot T_i(t_i, t_o, \sigma_w), \tag{2}$$

where

$$S_i(|\mathbf{x}_i - \mathbf{x}_s|, \sigma_i) = \frac{\kappa}{4\pi \sinh \kappa} \exp\left(\kappa \cos |\mathbf{x_i} - \mathbf{x_s}|\right) \tag{3}$$

and

$$T_i(t_i, t_o, \sigma_w) = \frac{1}{\sqrt{2\pi}\sigma_w} \exp\left(-\frac{(t_i - t_o)^2}{2\sigma_w^2}\right) \tag{4}$$

The spatial component of the signal p.d.f., S_i, is the Kent-Fisher distribution (Kent 1982), and it represents a slight deviation in the signal p.d.f. definition with respect to previous searches (see Aartsen et al. (2014b)). This function is analogous to a 2-dimensional Gaussian distribution, but it is normalized to the 2-sphere rather than an infinite plane. The concentration parameter κ is determined by the event angular uncertainty and is defined as $\kappa = \sigma_i^{-2}$. The temporal component of the signal p.d.f., T_i, is simply a Gaussian with mean emission time of t_o and a width of σ_w.

The background p.d.f., $\mathcal{B}_i$, is derived from the final level data set which is dominated by background. It has the following form

$$\mathcal{B}_i(\mathbf{x}_i, t_i) = P_{BkgDec}(\delta_i)\frac{P_{BkgAz}(\alpha_i)}{T}, \tag{5}$$

where T is the total livetime of the search, $P_{BkgDec}(\delta_i)$ is a p.d.f. describing the event declination distribution, and $P_{BkgAz}(\alpha_i)$ is a p.d.f. describing the event distribution in detector azimuth. These p.d.f.s are generated directly from data, without reference to background simulations.

The likelihood function itself is simply the product sum of all individual event probabilities:

$$\mathcal{L}(\mathbf{x}_s, n_s, t_0, \sigma_w) = \prod \mathcal{P}_i(|\mathbf{x}_i - \mathbf{x}_s|, n_s, t_i, t_0, \sigma_w, \sigma_i) \tag{6}$$

The ratio between the likelihood function values under the background only hypothesis ($n_s = 0$) and the signal plus background hypothesis is maximized by varying the source parameters n_s, σ_w, and t_0. The test statistic $\hat{\lambda}$ is then defined as the maximum value of the likelihood ratio:

$$\hat{\lambda} = -2\log\left[\frac{\sqrt{2\pi}\hat{\sigma}_w}{T}\frac{\mathcal{L}(n_s = 0)}{\mathcal{L}(\mathbf{x}_s, \hat{n}_s, \hat{t}_o, \hat{\sigma}_w)}\right] \tag{7}$$

303 with $\mathcal{L}(n_s = 0)$ corresponding to the likelihood of the null hypothesis and $\mathcal{L}(\mathbf{x}_s, n_s, \hat{t}_o, \hat{\sigma}_w)$

304 the likelihood of the signal plus background hypothesis with the best-fit values of the source

305 parameters. Because this is a search for sources of finite duration over a limited timescale,

306 the number of potential short duration flares within the data set exceeds that of flares of

307 longer duration, leading to an effective trials factor. This results in a bias towards flares of

308 shorter duration. We counteract this effect by introducing a marginalization term $T/\sqrt{2\pi}\hat{\sigma}_w$

309 in the test statistic formulation which serves to penalize flares of shorter duration. This

310 term also ensures that the test statistic will asymptotically follow a χ^2 distribution with

311 degrees of freedom corresponding to the number of fitted parameters for data consisting

312 solely of background events. More details about this term and its justification can be found

313 in Braun et al. (2010).

314   The χ^2 behavior of the test statistic enables the maximized value $\hat{\lambda}$ to be used to

315 estimate the pre-trials p-value of the best-fit flare through the invocation of Wilks's theorem

316 (Wilks 1938). Because this search attempts to maximize the signal hypothesis over the

317 whole Northern sky many times, the actual significance of a given flare must be adjusted to

318 account for the effective number of trials accrued during the sky scan. We use the procedure

319 detailed in Aartsen et al. (2015) that involves scrambling the event arrival times in the final

320 dataset, which also serves to scramble the event right ascension. The search is performed

321 on the randomized background data set and the p-value of the most significant flare in

322 the search is recorded. Many iterations are performed to build a distribution of p-values

323 which can then be compared to the p-value of the result from the real data. The fraction of

324 background trials that result in a p-value of equal or greater significance than the observed

325 p-value dictates the probability that the observed result is simply the consequence of a

326 random background fluctuation. This probability is referred to as the post-trials p-value and

327 it represents the true significance of the search result with proper trials factor correction.

328   In order to preserve generality, the presented search makes no use of information

329 outside of the data set to designate source regions or time periods of interest. Instead,

330 each point in the sky over a declination band ranging from -5° to 90° is examined. This

331 is accomplished by discretizing the sky into separate bins and letting the location of these

332 bins serve as the location of a hypothetical flaring source. Maximization of the likelihood is

333 then performed to obtain a test statistic $\hat{\lambda}$ for each bin. The first iteration of this scan uses

334 a relatively coarse 2° by 2° binning. After this first scan, a followup scan with finer 0.5° by

335 0.5° binning is performed over the coarse bins featuring a pre-trials p-value more significant

336 than a predefined threshold ($-\log_{10}$(p-value) > 1.75). The result is a map of pre-trials

337 p-values which shows the estimated significance of the best-fit flare hypothesis at each bin.

338 The best-fit flare from the bin featuring the most significant maximized test statistic after

339 both scans is returned as the hottest spot in the search.

4. Results and Interpretations

341   Applying the described analysis method to the unscrambled dataset yields the skymap

342 of the pre-trials p-values shown in Figure 3. The most significant flare is located at (RA,

343 Dec.) = (268.75°, 54.25°) with a signal strength n_s of 13.53 signal events and a width σ_w

344 of 5.89 days with the peak occurring on MJD 56107 (2012 June 29). The pre-trials p-value

345 for this flare is estimated at 6.68×10^{-5}. The post-trials probability of seeing such a flare

346 in a data set consisting of background only is 56%, indicating that this flare is entirely

347 consistent with the background hypothesis of the data. In light of this null result, we can

348 set an upper limit on the time-integrated neutrino flux of any possible unobserved neutrino

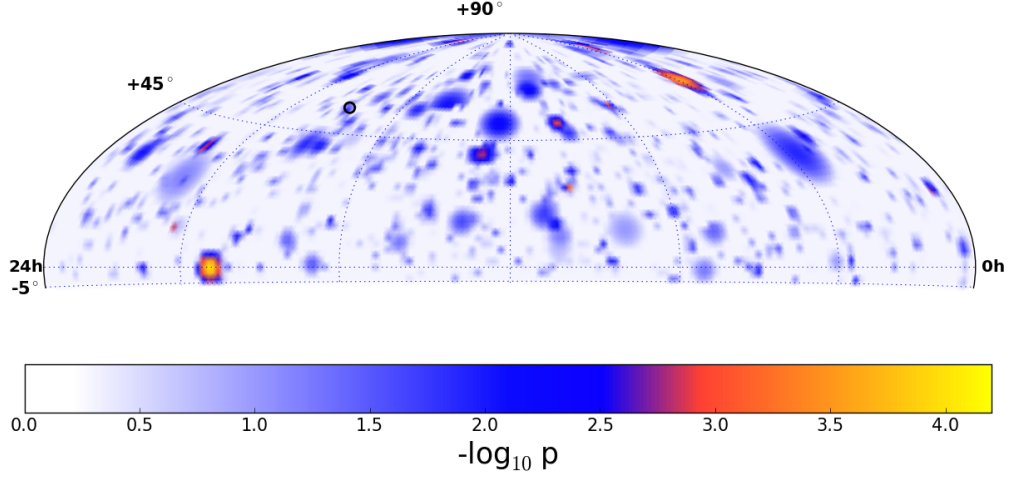349 flare that may have occurred during the search period.

Fig. 3.— Sky map of pre-trials p-values for best fit flares per bin. The black circle identifies the location of the most significant flare found at RA = 268.75° and Declination = 54.25° (Color version available online).

4.1. Generic Source Limit

Due to the focus on low-energy events in this search, we choose to examine the limit with respect to a soft-spectrum E^{-3} generic flaring neutrino source with a Gaussian emission profile. An upper limit is established through signal injections at a specified location through the following process. First, we select the p-value of the most significant flare found in the data to serve as a threshold for signal injection trials. Signal events are then injected with some Poisson mean value that is increased until the recovered p-values from the injections exceed the threshold p-value 90% of the time. This Poisson mean number of signal events is then taken as an event upper limit for the analysis method.

The upper limit on a generic flaring source for several emission timescales and choices of declination is plotted in Figure 4. The number of events required rises at longer timescales as the rate of accidental background correlations becomes non-negligible. The limit in terms

of time-integrated flux $(\mathrm{GeV^{-1}\cdot\,cm^{-2}})$ is also plotted. This limit is obtained by folding the source spectrum with the effective area of the event selection and normalizing the flux so that the number of events produced in the detector corresponds to the calculated Poisson mean event upper limit.
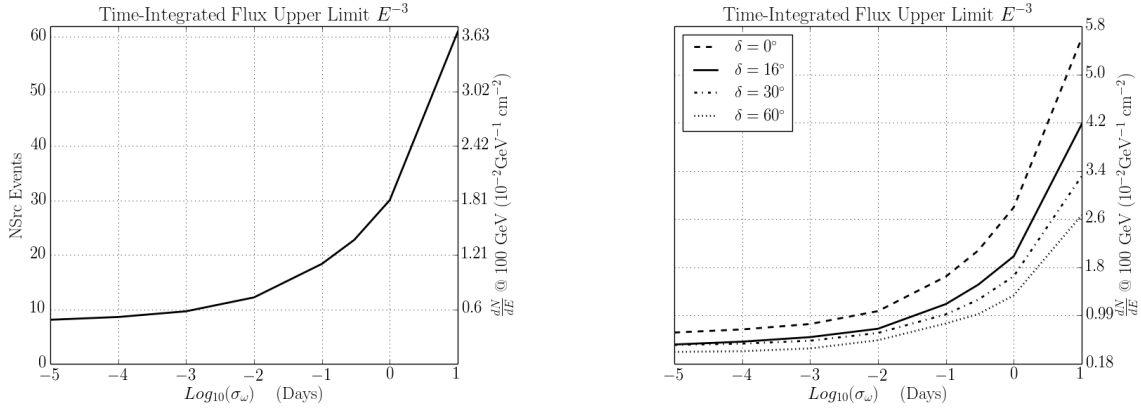
Fig. 4.— (left) Upper limit (90% C.L.) for a generic $\mathrm{E^{-3}}$ transient source as a function of flare width σ_w averaged over the declination range of the analysis. The limit is given in mean number of events (left axis) as well as in time-integrated flux at a reference energy of 100 GeV (right axis). (right) Upper limit (90% C.L.) for a generic $\mathrm{E^{-3}}$ transient source as a function of flare width σ_w for different values of source declination.

4.2.   Choked GRB Limits

This null result can also be used to construct limits on specific neutrino emission models such as the RMW/AB model for choked GRB emission mentioned previously. Unlike the hard spectra sources (e.g, $\mathrm{E^{-2}}$) that are the typical target in IceCube searches, the neutrino flux for choked GRBs is predicted to be much softer. The spectral shape can be modeled via a doubly broken power law with spectral breaks occurring as hadronic $(E_{\nu^{(1)}})$ and radiative $(E_{\nu^{(2)}})$ cooling mechanisms become efficient (see Eq. 8). Using the

canonical RMW/AB model parameters, the break energies for pions (kaons) occur at 30

GeV (200 GeV) and 100 GeV (20 TeV). Therefore the neutrino spectrum is predicted to be

very soft at $\gtrsim 1$ TeV energies.

$$\frac{d\Phi_\nu}{dE} = F_\nu \begin{cases} E^{-2} & E < E_\nu^{(1)} \\ E_\nu^{(1)} E^{-3} & E_\nu^{(1)} < E < E_\nu^{(2)} \\ E_\nu^{(1)} E_\nu^{(2)} E^{-4} & E_\nu^{(2)} < E < E_{max} \end{cases} \tag{8}$$

$$F_\nu = \frac{<n>_{\pi(K)} B_{\pi(K)}}{8} \cdot \frac{E_j \Gamma_b^2}{2\pi D^2 \ln(E'_{p,max}/E'_{p,min})} \tag{9}$$

The fluence F_ν at the Earth is given by Eq. 9 and depends upon the pion (kaon) multiplicity

$<n>$, the neutrino production branching ratio for pions (kaons) $B_{\pi(K)}$, the minimum and

maximum proton energies $(E'_{p,min}, E'_{p,max})$, the kinetic energy of the jet E_j, the bulk Lorentz

factor Γ_b, and lastly the distance to the source D. Equations 8 and 9 reveal that the

normalization of the neutrino flux at the Earth is highly dependent on the kinetic energy of

the jet E_j and the bulk lorentz factor Γ_b. These two parameters also determine the shape

of the spectrum as the hadronic ($E_{\nu^{(1)}} \propto E_j^{-1} \Gamma_b^5$) and radiative ($E_{\nu^{(2)}} \propto \Gamma_b$) break energies

depend upon these jet properties as well. We therefore choose to examine the predicted

neutrino fluence in E_j-Γ_b phase space.

To determine which values of these parameters produce a fluence detectable through

our search method, an event upper limit is first determined via the injection of signal events

following a spectrum set by the value of E_j and Γ_b (the same process used to calculate

event sensitivity for the generic E^{-3} scenario). This event upper limit is then combined

with the effective area of the event selection to determine the neutrino fluence necessary for

detection. For a given choice of E_j and Γ_b this sets a limit on the distance at which the

source would still be visible to the search, and we define this distance D_{vis} as the visibility

distance.

When combined with the area of sky examined by the search Ω_A, this visibility distance,

– 24 –

in turn, defines a parameter dependent volume V_A ($= \frac{1}{3}\Omega_A D_{vis}^3$) over which the search

method monitors. This monitored volume corresponds to the region in which a choked GRB

event should be visible to the presented search method with 90% confidence (assuming jet

alignment). If the observation period of the search is considered, this monitored volume can

be converted into a limit on the volumetric rate of choked GRB events as a function of E_j

and Γ_b. This, however, requires the assumption that the jets of any choked GRB event in

this volume are aligned with the Earth. To obtain a limit more representative of the actual

distribution of choked GRB orientations, one can include a geometrical correction factor

that takes into account the opening angle of the jets, θ_j, which is often approximated as

$\theta_j \sim \frac{1}{\Gamma_b}$ (Mizuta & Ioka 2013). Because the physics that determines this opening angle is

not entirely known, we choose not to include any correction for jet opening angle. The rate

limit is then given by

$$R = \left(\frac{U.L.(0|\mu)}{\tau \cdot V_A} \right), \tag{10}$$

where τ is the livetime of the search, V_A is the monitored volume previously defined, and

$U.L.(0|\mu)$ is the null observation upper limit on the number of choked GRBs that occurred

in our monitored volume with background expectation of μ.

We define this background expectation μ as the expected number of 'false positive'

flares that occur due to coincident background events during a given search. To calculate

the value of μ, we first perform many iterations of the analysis with n_s signal events injected

at a specific declination where n_s is the calculated event sensitivity at that declination.

The test statistic for these injection trials form a distribution from which we can take the

median value, λ_{inj}^{med}. Once λ_{inj}^{med} has been determined, the analysis is run again scanning

over the same declination band using a time-scrambled dataset with no injections. Several

iterations of this procedure builds a background test statistic distribution. The number of

entries in the background distribution whose test statistic value exceeds the threshold λ_{inj}^{med}

are then recorded. This number is then divided by the number of background-only analysis

420 iterations performed to yield an expected false positive rate per search. This procedure

421 revealed the false positive rate to be very small ($\leq 10^{-3}$). We therefore take $\mu \approx 0$ leading

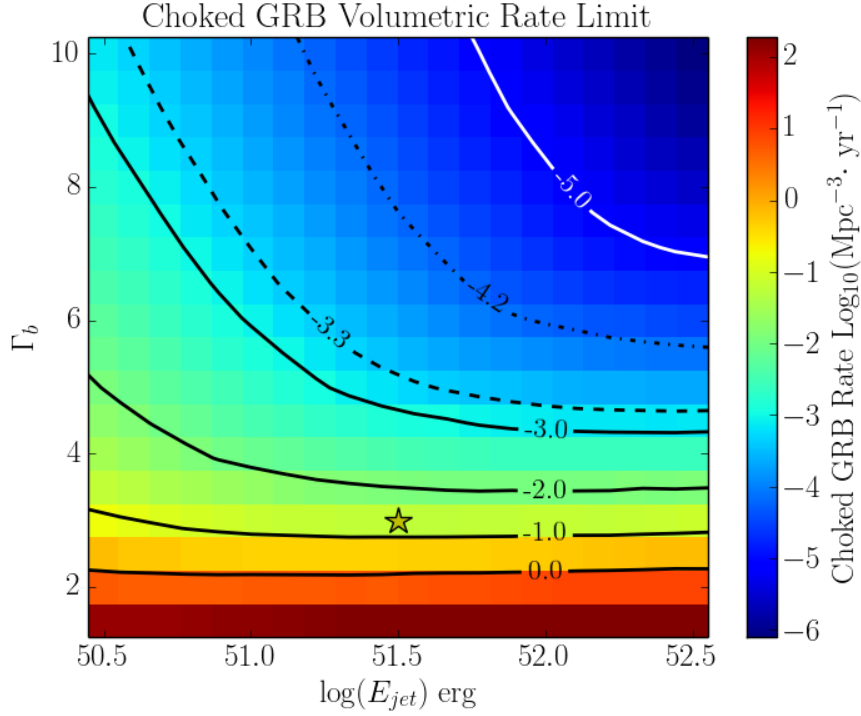to a Neyman upper limit of 2.3 from the null observation.

Fig. 5.— Histogram of the rate limit on choked GRBs in the nearby universe. The bin for canonical values of the RMW/AB emission model is marked by the star. The dashed line contour gives the rate of core-collapse supernovae within 10 Mpc as measured by Kistler et al. (2011). The dot-dashed line is the volumetric rate extracted from a large survey of SNe in the local universe (Leaman et al. 2011) (Color version available online)

422

423 The volumetric rate limit for a range of values of E_j and Γ_b is plotted in Figure 5.

424 Two separate measurements of the nearby CC SNe are plotted as well to provide context

425 to the calculated rate limits. Choked GRB events harboring particularly energetic jet

426 parameters should be visible to the search method. However, if one compares the limits for

427 the canonical RMW/AB model parameter values ($\Gamma_b = 3$, $E_j = 10^{51.5}$ erg) to the CC SNe

428 rates, it is clear that the current search method is not very sensitive to large regions of the

429 model parameter space. However, the sensitivity of this search can be improved through

430 refinement of the event selection and analysis methods. Potential changes include greater

431 signal retention through more efficient use of multi-variate machine learning cuts in the

432 event selection process, the use of reconstruction methods optimized for sub-TeV muon

433 tracks, and more accurate modeling of event angular error distribution.

5. Conclusions

435 The described search examined a newly developed data set consisting of 30-300 GeV

436 muon neutrinos. No evidence for transient astrophysical neutrino sources was found in the

437 data, leading to the construction of upper limits on the neutrino fluence of potential sources

438 within the observation period. In particular, we examine the derived limit in the context

439 of neutrino emission from choked GRBs. Although this search in its current configuration

440 is only sensitive to particularly energetic or nearby choked GRBs, the sensitivity of this

441 method will improve as the event selection and search techniques are further optimized for

442 muon neutrino events at sub-TeV energies. Continued development of this event selection

443 will complement the current mature IceCube analyses at higher energies, leading to an

444 overall enhancement of the detector's sensitivity to transient sources.

REFERENCES

Aartsen, M. G., Abbasi, R., Abdou, Y., et al. 2014a, Nuclear Instruments and Methods in Physics Research A, 736, 143

Aartsen, M. G., Ackermann, M., Adams, J., et al. 2014b, ApJ, 796, 109

Aartsen, M. G., Ackermann, M., Adams, J., et al. 2015, The Astrophysical Journal, 807, 46

Abbasi, R., Abdou, Y., Abu-Zayyad, T., et al. 2012, Astroparticle Physics, 35, 615

Adrián-Martínez, S., Samarai, I. A., Albert, A., et al. 2012, ApJ, 760, 53

Ahrens, J., Bai, X., Bay, R., et al. 2004, Nuclear Instruments and Methods in Physics Research A, 524, 169

Ando, S., & Beacom, J. F. 2005, Physical Review Letters, 95, 061103

Becker, J. K., & Biermann, P. L. 2009, Astroparticle Physics, 31, 138

Braun, J., Baker, M., Dumm, J., et al. 2010, Astroparticle Physics, 33, 175

Braun, J., Dumm, J., De Palma, F., et al. 2008, Astroparticle Physics, 29, 299

IceCube Collaboration, Achterberg, A., Ackermann, M., et al. 2006, Astroparticle Physics, 26, 155

Kent, J. T. 1982, Journal of the Royal Statistical Society. Series B (Methodological), 44, pp. 71

Kistler, M. D., Yüksel, H., Ando, S., Beacom, J. F., & Suzuki, Y. 2011, Phys. Rev. D, 83, 123008

Leaman, J., Li, W., Chornock, R., & Filippenko, A. V. 2011, Monthly Notices of the Royal Astronomical Society, 412, 1419

Mészáros, P., & Waxman, E. 2001, Physical Review Letters, 87, 171102

Mizuta, A., & Ioka, K. 2013, ApJ, 777, 162

Modjaz, M. 2011, Astronomische Nachrichten, 332, 434

Murase, K., Kashiyama, K., & Mészáros, P. 2013, Physical Review Letters, 111, 131102

Neunhöffer, T. 2006, Astroparticle Physics, 25, 220

Razzaque, S., Mészáros, P., & Waxman, E. 2004, Physical Review Letters, 93, 181101

Rees, M. J., & Meszaros, P. 1992, Monthly Notices of the Royal Astronomical Society, 258, 41P

Taboada, I. 2010, Phys. Rev. D, 81, 083011

Thrane, E., Abe, K., Hayato, Y., et al. 2009, ApJ, 704, 503

Whitehorn, N., van Santen, J., & Lafebre, S. 2013, Computer Physics Communications, 184, 2214

Wilks, S. S. 1938, Ann. Math. Statist., 9, 60

Woosley, S. E., & Bloom, J. S. 2006, Annual Review of Astronomy & Astrophysics, 44, 507